ANGLE- AND SPIN-RESOLVED PHOTOELECTRON SPECTROSCOPY

U. Heinzmann

Fakultät für Physik
Universität Bielefeld
D - 4800 Bielefeld, F.R.G.

INTRODUCTION AND GENERAL COMMENTS

Experimental analysis of the photoelectron-spin polarization vector in photoionization using circularly polarized light (Fano effect[1]) was up to 1984 restricted to angle-integrated measurements[2] without resolution of the kinetic energy of the photoelectrons corresponding to different ionic states. With the development of the new German dedicated electron storage ring for synchrotron radiation BESSY in Berlin, a light source of circularly polarized vacuum ultraviolet (vuv) radiation with sufficiently high intensity has become available, which makes angle- and energy-resolved spin-polarization transfer studies from circularly polarized radiation onto photoelectrons feasible. These measurements could be performed with free atoms,[3,4] atoms adsorbed on solid surfaces[5,6] as well as with a solid state system[7] even in a photon energy range $\geq$ 10 eV, where conventional methods for producing circularly polarized radiation break down because no transparent or even double refracting material exists. These studies using circularly polarized radiation complement recent photoelectron spectroscopy measurements with free randomly oriented[8] as well as free oriented molecules[9]. One of the reasons why these experiments have been done is to find a set of parameters measured in the experiments which characterize the photoemission process quantummechanically completely. It builds a bridge from the atoms via the molecules via the adsorbates up to the three dimensional solid state and makes this cross comparison not only in terms of intensities and polarizations but also by means of dipole matrix elements and phase shift differences of continuum wave functions for single channels, which are energy degenerate but have been isolated by the data-combination of different non-redundant experiments.

The reaction plane of symmetry for an angle- and spin-resolved photoionization process of an unpolarized atom or unoriented molecule using circularly polarized radiation is shown in Fig. 1. Because the momentum of the photon is negligibly small compared with the momentum of the photoelectron (valid in nonrelativistic approximation if photon energy $\lesssim$ 100 eV) there is a forward-backward symmetry in the reaction plane of Fig. 1. It also makes no difference whether right handed circularly polarized radiation comes from the left or left handed comes from the right. The rotational symmetry around the direction of the photon momentum causes, that both electron spin polarization components perpendicular to the photon spin have to vanish for photoelectron emission angles $\theta = 0, \pi/2, \pi$. This is shown in Fig. 2, where the angle dependences of intensity $I(\theta)$ and spin polarization components are shown for a certain atomic photoionization process, which has been simultaneously resolved with respect to all variables one has: radiation wavelength 80 nm, radiation polarization σ^+, electron emission angle θ, electron kinetic energy corresponding to the final ionic state $Xe^+ {}^2P_{1/2}$, the 3 components of the electron spin polarization vector $\vec{P}(\theta)$: $P_\perp(\theta)$ perpendicular to the reaction plane, $A(\theta)$ parallel to the photon spin, $P_p(\theta)$ perpendicular to the photon spin but in the reaction plane.

The curves in Fig. 2 are fits to the experimental points[3,10] (the size of a typical error-bar cross is given in the middle part) and are in accordance with the theoretical predictions by Cherepkov[11] and Lee[12]:

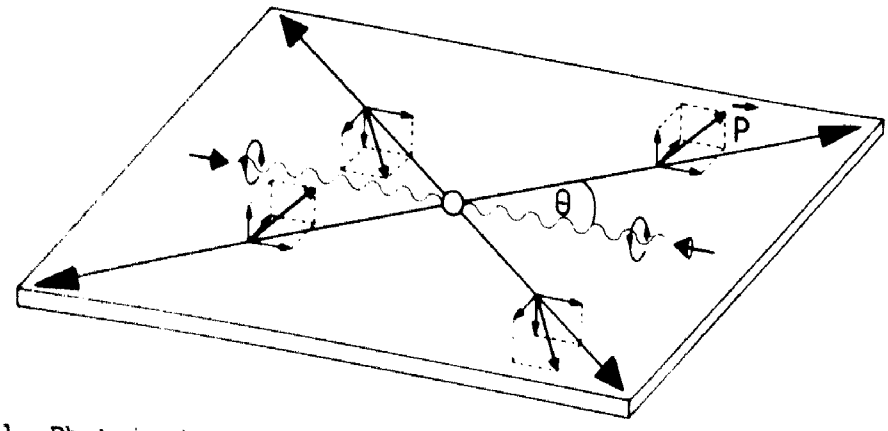

FIG. 1. Photoionization reaction plane using circularly polarized radiation. The results do not depend on whether right handed circularly polarized light comes from the left or left handed comes from the right.

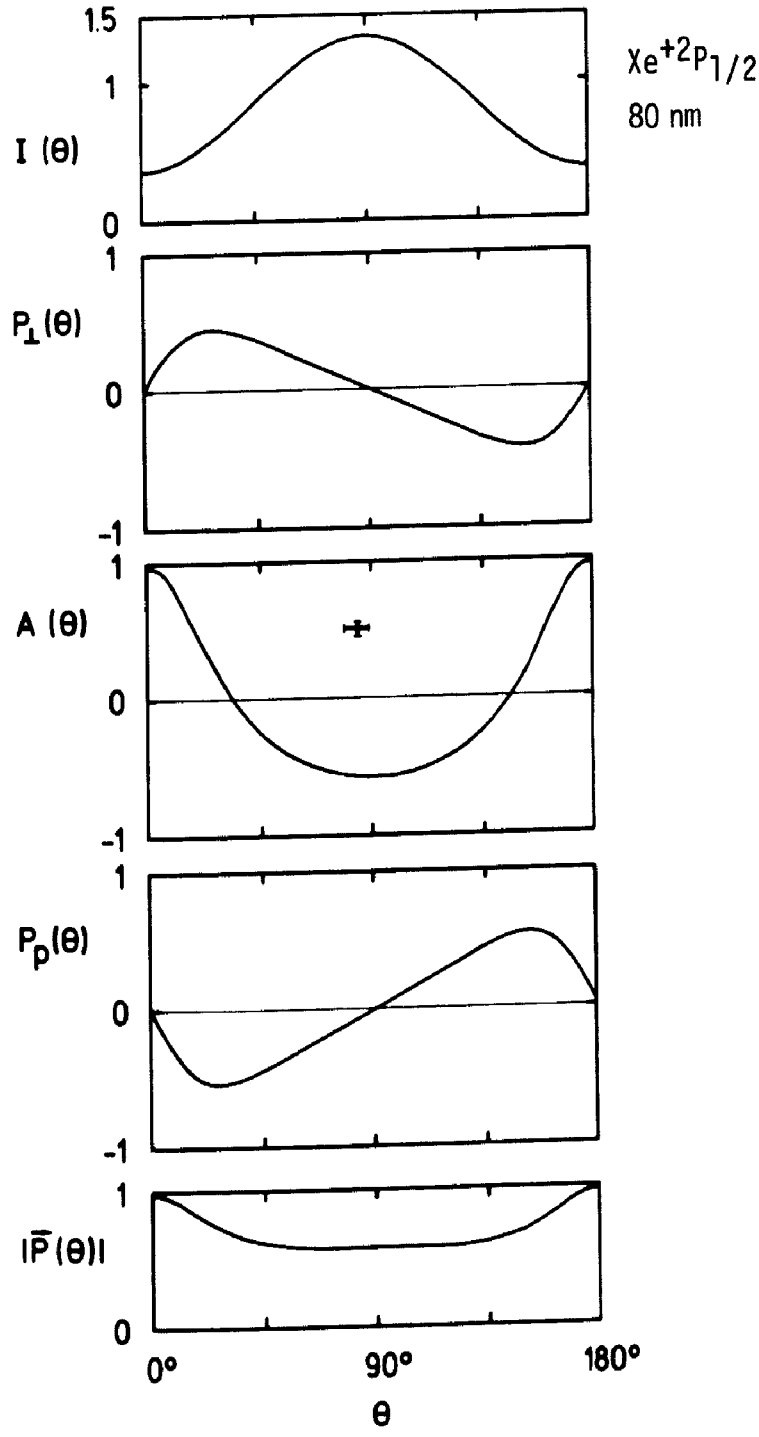

FIG. 2. Fit-curves of the experimental results (the size of a typical error-bar cross is given in the middle part) describing the angular dependences of the photoelectron intensity $I(\theta)$, of the 3 components and the length of the spin-polarization vector for photoionization of Xe atoms using radiation of 80 nm corresponding to photoelectrons leaving the ion in the $^2P_{1/2}$ state.[3]

$$I(\theta) = 1 - \frac{\beta}{2}\left(\frac{3}{2}\cos^2\theta - \frac{1}{2}\right)$$

$$P_{\perp}(\theta) = 2\,\xi \sin\theta\cos\theta\,/I(\theta)$$

} independent on helicity of light

$$A(\theta) = \pm\left(A - \alpha\left(\frac{3}{2}\cos^2\theta - \frac{1}{2}\right)\right)/I(\theta)$$

$$P_p(\theta) = \pm\,\alpha \sin\theta\cos\theta\,/I(\theta)$$

} + for σ^+ light, - for σ^- light

β, ξ, A, α and the total photoionization-cross section Q are the so called dynamical parameters of the photoionization process, which are energy dependent and which are one possible set for a complete quantummechanical characterization.

$A(\theta)$ and $P_p(\theta)$ vanish, if linearly polarized or unpolarized instead of circularly polarized radiation is used.[13,14] All five curves in Fig. 2 show a mirror symmetry with respect $\theta = \pi/2$, but $P_{\perp}(\theta)$ and $P_p(\theta)$ with changing sign. Thus, the polarizations of opposite sign cancel one another, if the photoelectrons ejected are extracted by an electric field regardless of their direction of emission. The only non-vanishing component of the spin polarization in an angle-integrated measurement is $A(\theta)$ which yields A as the average value. This Fano-effect value A is identical with $A(\theta)$ for the so called magic angle $\theta = 54°$, where the second Legendre polynomial vanishs. To determine A in an angle resolved experiment yields the advantage, that it can be now also studied as function of the electron energies by use of an electron spectrometer in the experiment, which was impossible in the former original type of experiment to determine A angle integrated. It is also worth noting that within the error limits the photoelectrons emitted into forward direction $\theta = 0$ have been found[3] to be completely spin polarized (Fig. 2 middle part), which has been explicitly theoretically predicted for this final ionic state one and a half decades ago.[15] This complete electron-spin polarization in forward direction parallel to the photon spin as well as the fact, that the electron polarization is proportional to the degree of photon polarization if partly polarized radiation is used, allows to use the headline "spin-polarization transfer" from spin polarized photons onto photoelectrons to characterize the process.

The lowest part of Fig. 2 demonstrates that the length of the electron-polarization vector never vanishs as function of the emission angle θ. This can be generalized by the experimentally improved rule, that in an angular resolved photoemission experiment on atoms, molecules, adsorbates or solid states it is rather very common than exceptional to get spin polarized photoelectrons.

EXPERIMENTAL TECHNIQUES

The main components of the two apparatus we have built up at the new German electron storage ring BESSY - one for the studies of atomic and molecular photoionization[3] and one for photoemission experiments with solid surfaces[7] and adsorbates[5] - are briefly discussed here; they are partly shown in Fig. 3. The synchrotron radiation is dispersed by a 6.5 m N.I. UHV monochromator of the Gillieson type[16], not shown in Fig. 1, with the electron beam in the storage ring being the virtual entrance slit. A spherical mirror and a plane holographic grating (1200 lines/mm) form a 1 : 1 image of the tangential point in the exit slit. With a slit width of 2 mm a bandwidth of 0.5 nm has been achieved. Apertures movable in vertical direction are used to select radiation emitted above and below the storage ring plane, which has positive or negative helicity, respectively. In the plane, the synchrotron radiation is linearly polarized.

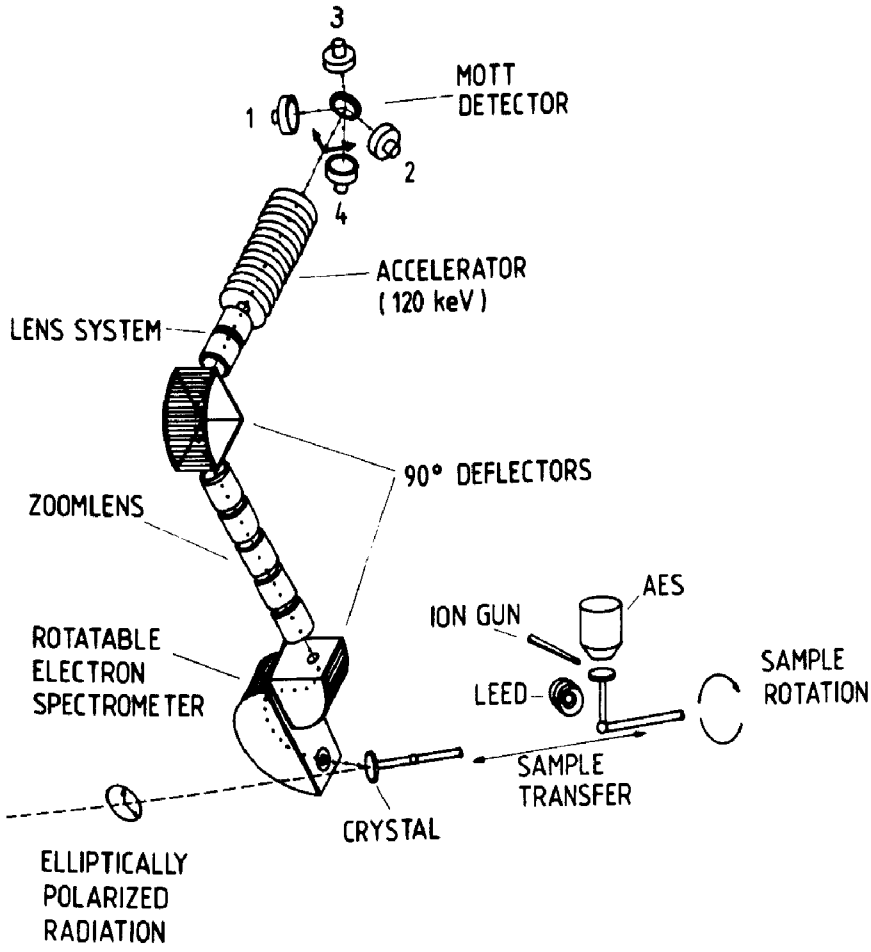

FIG. 3. Schematic diagram of the apparatus, built up at BESSY,[7] shown for the general case of off-normal photoemission.

The monochromatized and in general elliptically polarized light hits the target (crystal, atomic beam) producing photoelectrons in a region free of electric or magnetic fields. The photoelectrons emitted in the reaction plane at an angle θ are energy analyzed in a simulated hemispherical electron spectrometer[17], which is rotatable around the normal of the reaction plane. An electrostatic deflection by 90° directs the electron beam along the axis of rotation of the electron spectrometer. After a second deflection by 90° the electron beam is accelerated to 120 keV and scattered at the gold foil of the Mott detector[18]. $A(\theta)$ and $P_{\perp}(\theta)$ both being transverse components, are simultaneously determined from the left-right scattering asymmetry measured by two pairs of detectors as shown in Fig. 3. Instrumental asymmetries could be easily eliminated by taking advantage of the reversal of light helicity and of the change of the emission angle from θ to $-\theta$ as well as by use of 4 additional detectors in forward scattering directions in the Mott detector, not shown in Fig. 3.

In the solid state apparatus, the sample is cleaned by ion bombardment, heating in oxygen, and flashing; it is characterized by low energy electron diffraction (LEED) and scanning Auger electron spectroscopy in a separate preparation chamber. The crystal on top of a three-axes manipulator moveable between preparation and photoemission chamber, can be cooled by use of a temperature-controlled liquid He-Cryostat to temperatures of less than 40 K. The adsorbate is introduced via a doser nozzle which kept the background pressure below 10^{-9} mbar (base pressure $5 \cdot 10^{-11}$ mbar), allowing the continuous monitoring of the photoelectron spectra and LEED pattern as function of coverage. The photoelectrons emitted into a cone ±3° are energy analyzed at a resolution of 90 meV FWHM.

The optical degrees of polarization of the synchrotron radiation have been measured[3] by means of a rotatable four mirror analyzer[19] not shown in Fig. 3. Fig. 4 shows the results for the circular polarization P_{circ} and the linear polarization P_{lin} as functions of the vertical angle Ψ (±0.1 mrad). The solid lines which represent the theoretical predictions according to Schwinger's theory and which show excellent agreement with the experimental points (error-bar crosses) demonstrate a complete linear polarization and a vanishing circular polarization of radiation emitted in the plane of the BESSY-storage ring. Fig. 5 shows the integrated results for the case the vertical angular ranges are from Ψ to ±5 mrad. The photoelectron spinpolarization spectroscopy studies have been performed with P_{circ} = 95 % and P_{lin} = 31 %. Under these conditions a photon flux of a few $10^{11} s^{-1}$ passes the monochromator exit slit and hits the phototarget. Typical count rates in the Mott detector were a few s^{-1} for gas phase experiments and $10^{3} s^{-1}$ for studies with solids and adsorbates.

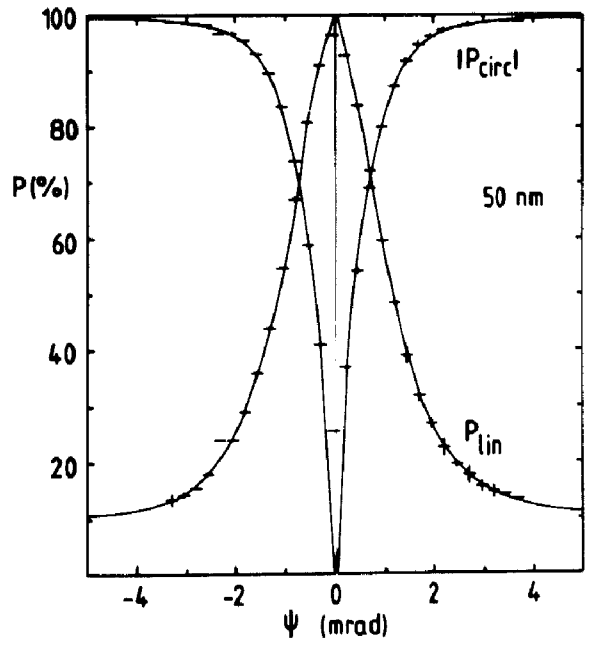

FIG. 4. Degree of circular and linear polarization P_{circ} and P_{lin}, respectively, of vuv synchrotron radiation emitted from the BESSY storage-ring plane as function of the vertical angle ψ (± 0.1 mrad).[3]

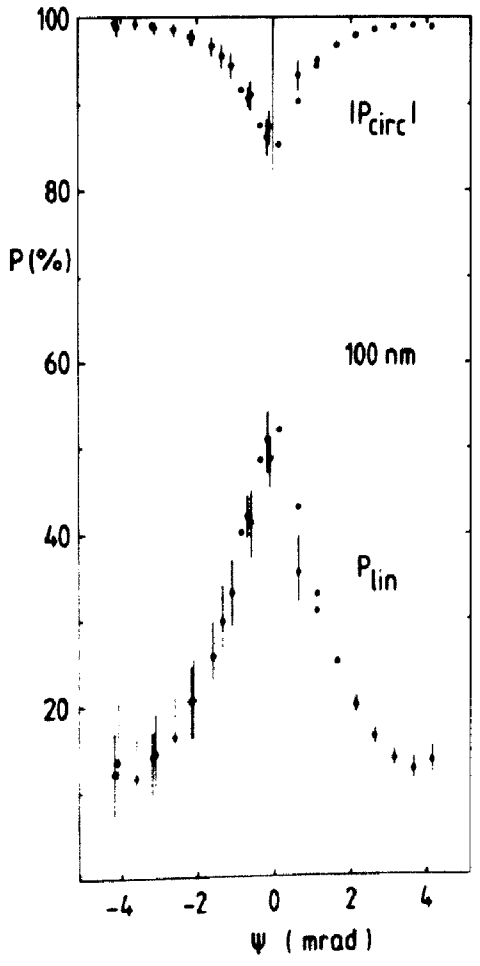

FIG. 5. As Fig. 4 but integral in a vertical angular range from ψ to ± 5 mrad.[3] The wavelength dependence of P_{circ} and P_{lin} between 50 and 100 nm is the same within the experimental uncertainties.

All photoelectron spin polarization effects in atoms arise due to the existence of the spin-orbit interaction. Because of that the ℓ and m_ℓ quantum numbers are no longer good and thus the "spin momentum transfer" is no longer performed from the photon spin to the orbital angular momentum ℓ and m_ℓ but to the total angular momentum j and m_j of which the photoelectron spin is a part. Discussing this influence of the spin-orbit interaction quantitatively, however, one has to distinguish between two cases, which will be discussed in this chapter at certain examples in detail:

1. Photoionization of atoms, where the discrete atomic or ionic states involved show a fine structure splitting induced by the spin-orbit coupling.
2. Photoionization of an atomic s-subshell, where neither the ground-state nor the final ionic state shows a splitting.

Case 1 is fulfilled for photoionization of rare gase atoms; Fig. 6 shows the photoelectron spectrum of argon.[20] The two peaks correspond with the ionic states $^2P_{1/2}$ and $^2P_{3/2}$ of Ar^+, split by the existence of the spin-orbit interaction. Both peaks in the spectrum yield spin polarized photoelectrons but with a spin-polarization degree of opposite sign. Or otherwise, in the case

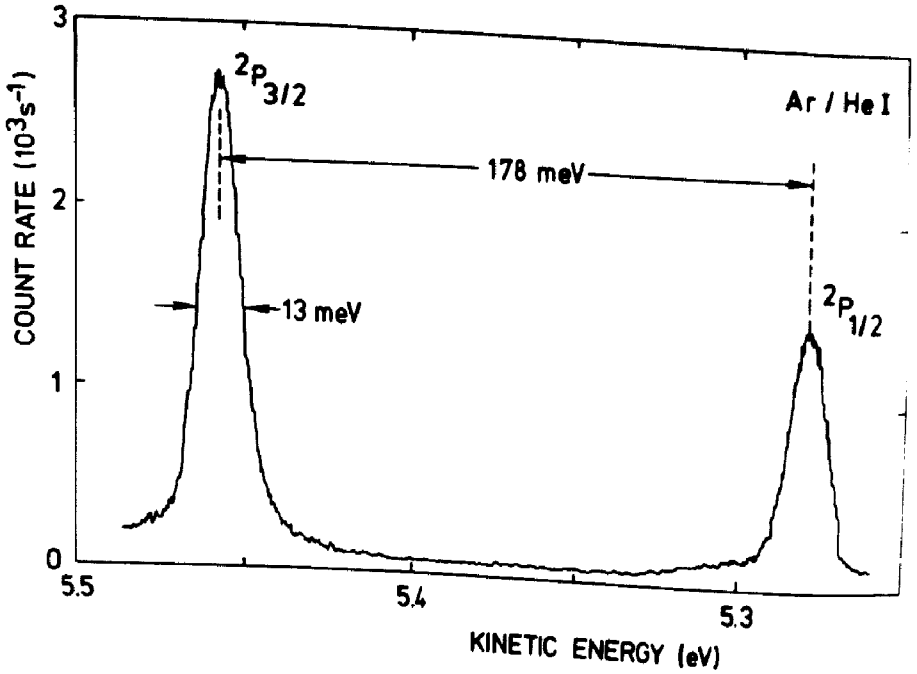

FIG. 6. Photoelectron spectrum of free argon atoms[20] using HeI vuv radiation (21.22 eV) and a simulated hemispherical electron spectrometer[17].

the spin-orbit interaction is not resolved by use of an appropriate electron spectrometer, the polarizations of opposite sign for both unresolved peaks would almost cancel one another. A quantitative example is shown in Fig. 7 as the wavelength dependences of the dynamical spin parameters α and A for photoionization of xenon. The agreement of the experimental data (error bars[3]) with the theoretical predictions (RRPA solid curves[21], RPAE dashed curve[22]) is good.

One needs the spin-orbit interaction and its resolved splitting in Fig. 6 in order to get polarized photoelectrons. It is, however, worth noting that the magnitude of the electron-spin polarization

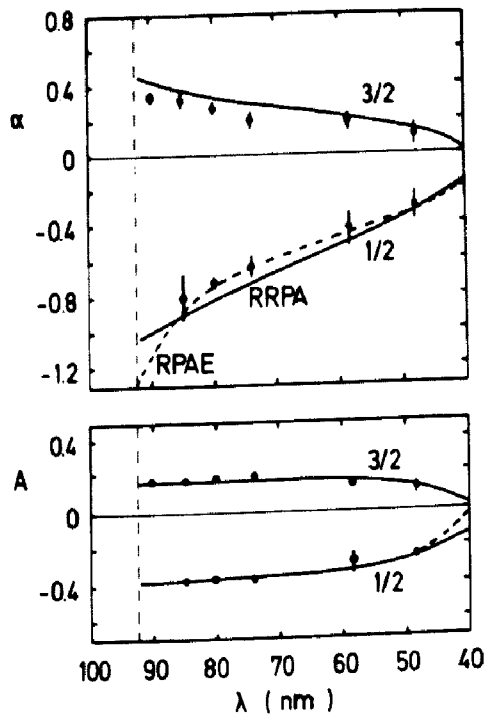

FIG. 7. Experimental results of the spin parameters α and A,[3] upper and lower part, respectively, as functions of the radiation wavelength for photoelectrons leaving the xenon ion in the $^2P_{3/2}$ and $^2P_{1/2}$ final states in comparison with theoretical predictions: RRPA[21], solid curve; and RPAE[22], dashed curve.

in both peaks does not depend on whether the spin-orbit interaction is strong or weak. While the fine-structure splitting in Xe^+ is seven times larger than in Ar^+, the magnitudes of the polarizations given by height and shape of the wavelength dependence of the dynamical spin parameter ξ shown in Fig. 8 are nearly the same for Ar, Kr and Xe. The only main difference in the three parts of Fig. 8 results in the different photoionization thresholds which shift the curves horizontally. Curves follow from calculations using RRPA (solid[23]), RPAE (dotted[22]) and MQDT (chained[19,24]).

Case 2 is discussed for the photoionization of mercury atoms as example:

$$Hg\ 6s^2\ (^1S_0) \longrightarrow Hg\ 6s\ (^2S_{1/2})\varepsilon p \begin{cases} ^1P_1 \\ ^3P_1 \end{cases}$$

The photoionization transitions into the two energy degenerate continuum final states $^1P_1$ and $^3P_1$ are described by the singlet and triplet amplitudes D_S and D_T, respectively, as well as by the difference of the continuum-phase shifts $\delta_S - \delta_T$. In terms of the transition amplitudes and phases, the dynamical parameters read[12,25,26]:

$$Q = \tfrac{4}{3}\pi^2 \alpha a_0^2 \omega (D_S^2 + D_T^2)$$

$$\beta = \frac{2D_S^2 - D_T^2}{D_S^2 + D_T^2}$$

$$\xi = \frac{3\sqrt{2} D_S D_T \sin(\delta_S - \delta_T)}{4(D_S^2 + D_T^2)}$$

$$A = \frac{D_T^2 - 2\sqrt{2} D_S D_T \cos(\delta_S - \delta_T)}{2(D_S^2 + D_T^2)}$$

$$\alpha = \frac{-D_T^2 - \sqrt{2} D_S D_T \cos(\delta_S - \delta_T)}{D_S^2 + D_T^2}$$

It is remarkable that the asymmetry parameter β depends incoherently upon the matrix elements with the consequence that neglecting the spin-orbit interaction ($D_T \equiv 0$) the "parity-favored" transition D_S yields $\beta = 2$. The spin parameter ξ is given by a single interference term containing the sine of the phase shift difference. It is worth noting, that all 3 spin-parameters ξ, A, α which are a measure for the 3 components of the spin-polarization vector are proportional to the "parity-unfavored" matrix element D_T. This means, that in this case the magnitude of the electron polarization is a measure of the strength of the spin-orbit interaction,

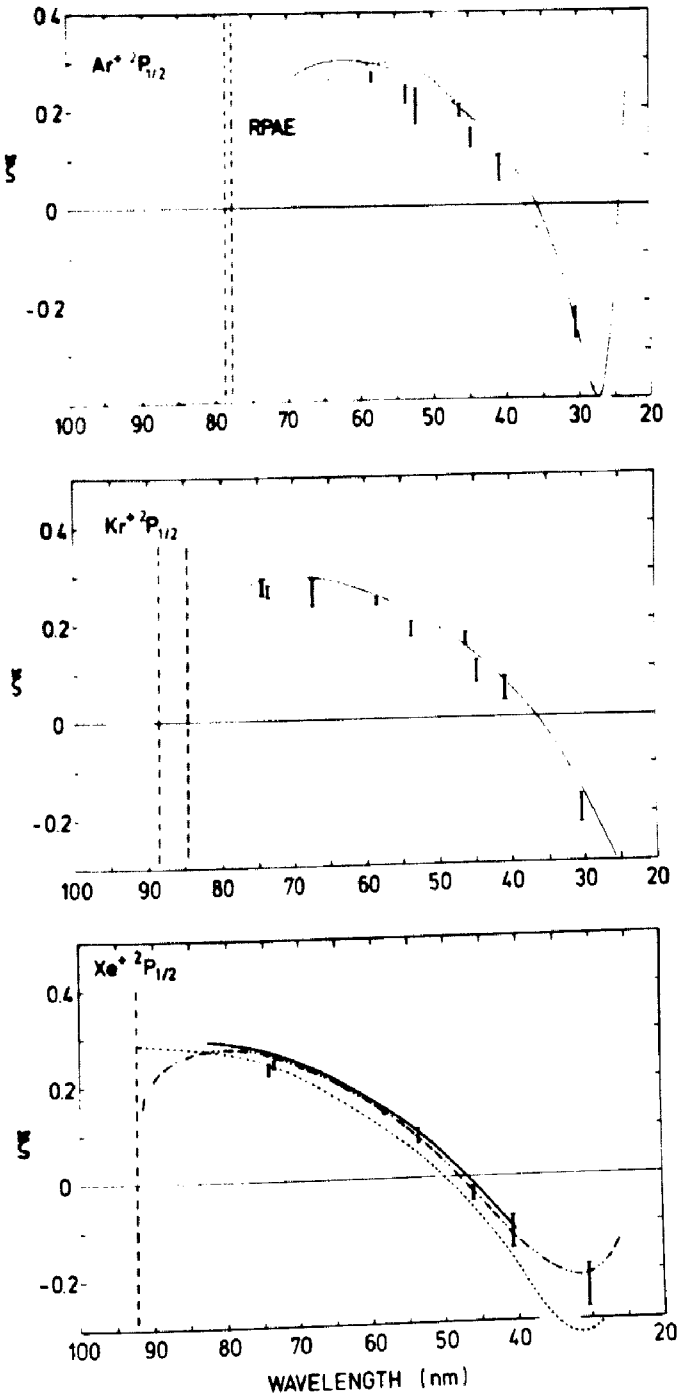

FIG. 8. Experimental results (error bars) of the spin parameter ξ for photoelectrons corresponding to the ionic state $^2P_{1/2}$ of Ar[13] (upper part), Kr[13] (middle part) and Xe[13,19] (lower part) in comparison with theoretical curves RRPA[23] (free), RPAE [22](dashed), MQDT[19,24] (chained). The vertical dashed lines represent the ionization thresholds.

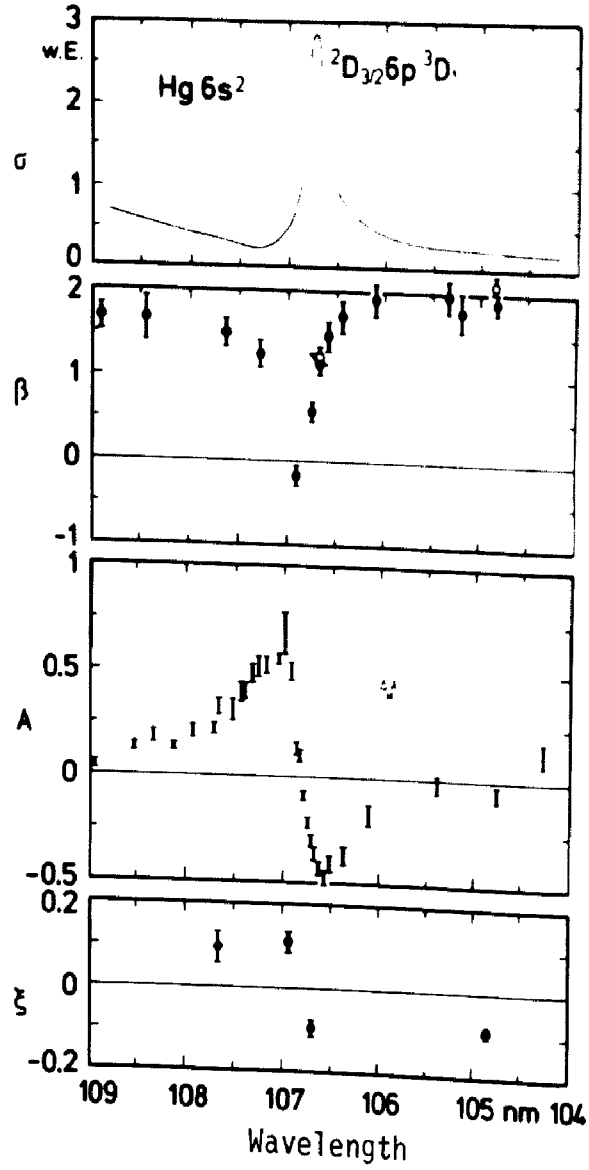

FIG. 9. Photoionization of mercury $6s^2$ in the autoionization region; cross section (upper part)[27]; asymmetry parameter β[28,29], spin parameters A and ξ[30].

which influences the photoionization process here in the final continuum state without a fine-structure splitting. Neglecting the spin-orbit coupling, all three spin parameters must vanish.

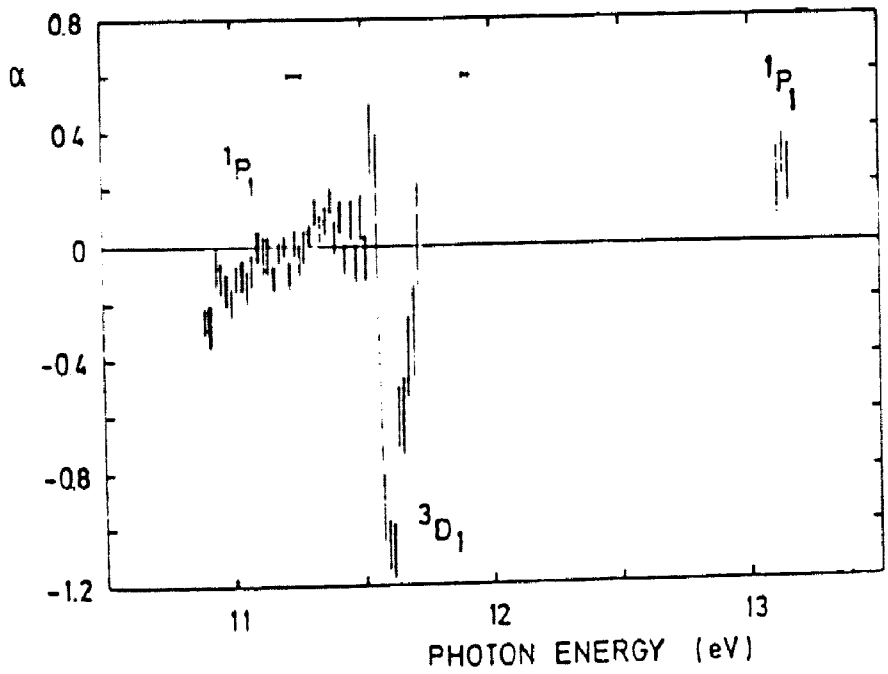

FIG. 10. The same as Fig. 9 but spin parameter α^{31}.

A strong enhancement of the influence of the spin-orbit interaction and thus a pronounced photoelectron-spin polarization has been seen in resonance regions, where effects of configuration interaction, channel mixing and many electron correlations play an important role. Fig. 9 and 10 give an example for the photoionization of mercury $6s^2$ in the autoionization region (via a virtual excitation of the $5d^{10}$ subshell into $5d^9 6p$) with respect to total photoionization cross section[27], the asymmetry parameter β[28,29], the spin parameters A^{30}, ξ^{30} and α^{31}, respectively. All 5 dynamical parameters show a pronounced variation as function of the wavelength.

The combination of the data given in Figs. 9 and 10 allows to determine the matrix elements D_S and D_T as well as the phase-shift difference $\delta_S - \delta_T$ separately; the results[31] are shown in Fig. 11; the error bars contain the uncertainties of all experimental quantities involved. The singlet and triplet amplitudes show quite different behavior: the parity favored D_S follows the shape of the cross section and is always different from zero, whereas the unfavored D_T exhibits three changes of sign. In the two $^1P_1$ resonances, the phase difference (lower part of Fig. 11) varies only weakly across these resonances. For the $^3D_1$ resonance, however, we find completely different conditions. Here the triplet amplitude is negative and the phase shift difference between the singlet and triplet partial continuum waves shows a sudden change of sign which is typical for the variation of a relative phase across a resonance.

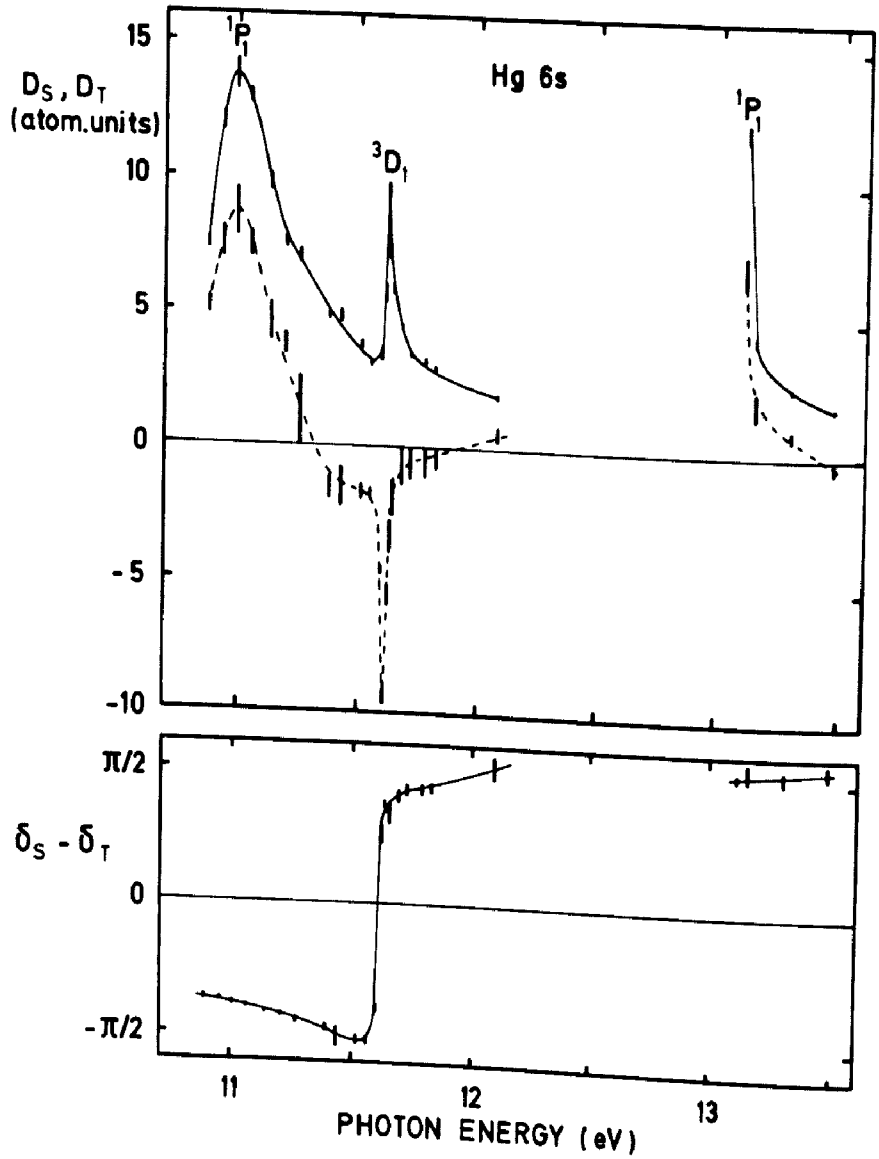

FIG. 11. Singlet and triplet matrix elements D_S and D_T (upper part) and corresponding phase shift difference (lower part)[31] obtained by use the data shown in Figs. 9 and 10. (curves: to guide the eyes).

In the same way as for the s-subshell of Hg the photoionization of atoms can also be characterized in terms of matrix elements and phase-shift differences in the case the ions show a fine structure splitting. But then, as discussed, the influence of the spin-orbit interaction onto the phases is in general a weak effect as for example seen in Fig. 12 showing the phase-shift difference between εf and εp partial waves in photoionization of the d subshell of Hg.[32] The full and open points with error bars correspond to the ionic states $^2D_{5/2}$ and $^2D_{3/2}$, respectively. The main contri-

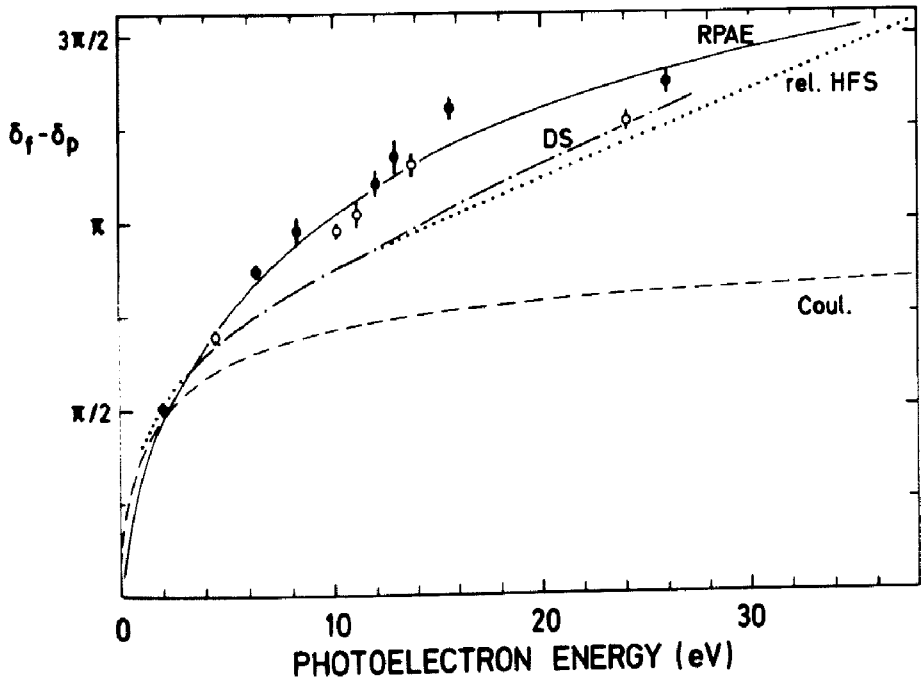

FIG. 12. Phase-shift difference between the εf and εp partial wave[32] in Hg 5d photoionization; full and open symbols correspond to the ionic states $^2D_{5/2}$ and $^2D_{3/2}$, respectively. Theoretical predictions Coulomb-phase difference $\sigma_f - \sigma_p - \pi$, relativistic Hartree Slater[33], Dirac Slater[34], RPAE with intertransition correlations between 5d → εp and 5d → εf.[35]

bution of the phase-shift difference especially close to the threshold comes from the Coulomb-phase shift, which varies by π/2 within 2.3 eV kinetic energy above the threshold. At higher energies effects of interchannel coupling play an important role as the comparison of the experimental data in Fig. 12 with the theoretical curves (rel. HFS[33], DS[34], RPAE[35]) shows.

The influence of parity-unfavored transitions is not only an important effect in autoionization resonances as discussed in Fig. 11 but also close to a Cooper minimum, where one matrix element changes its sign as function of the photon energy. This is the case for the $5p_{3/2}$ - $\varepsilon d_{3/2}$ transition at xenon.[10,36] The corresponding parity unfavored matrix element[4], which is a measure for the influence of the spin-orbit interaction, shows a pronounced enhancement as Fig. 13 upper part demonstrates, which is not seen in any corresponding parity favored matrix element. The phase shift (lower part Fig. 13) of the unfavored transition with reference to the phase of the favoured $5p_{3/2}$ - $\varepsilon s_{1/2}$ transition of xenon is very constant as function of the photon energy.

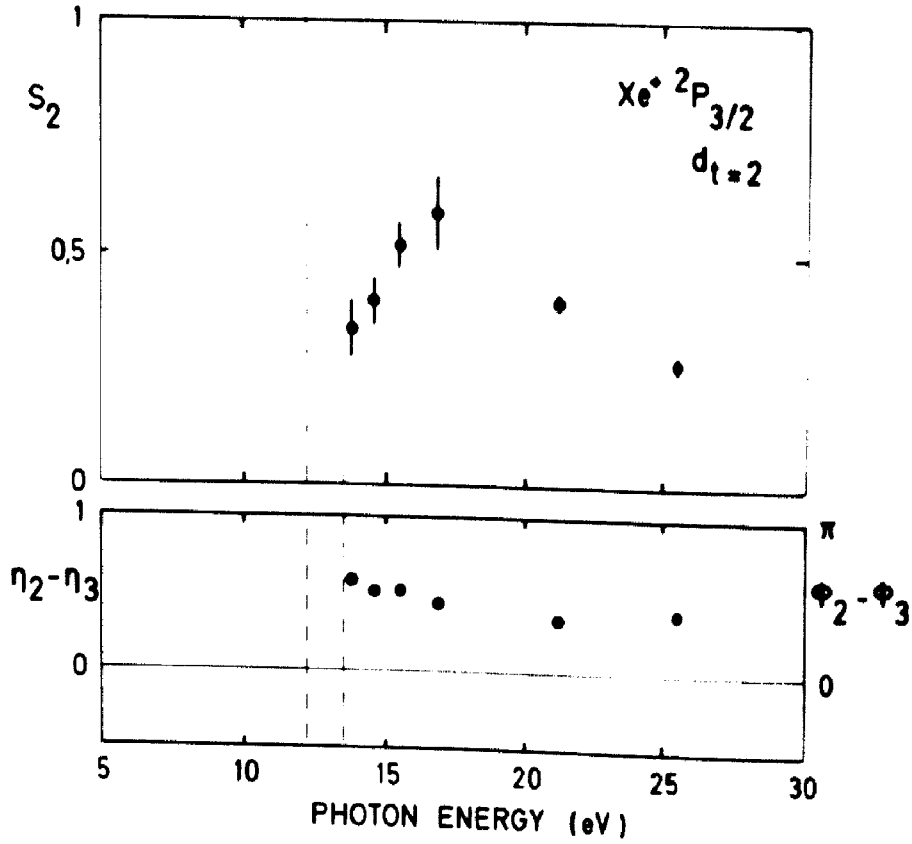

FIG. 13. Parity unfavored 5p → εd photoionization transition of Xe describing the strength of the influence of the spin-orbit interaction.[4] Upper part: reduced dipole-matrix element; Lower part: phase shift of the unfavored transition with reference to the phase of the favored s-transition. The dashed vertical lines represent the ionization thresholds.

MOLECULAR PHOTOIONIZATION

In molecular photoionization one has to take into account that the intramolecular Coulomb interaction is usually much stronger than the spin-orbit interaction. Therefore, it was believed over a period of several years that an electron polarization cannot occur in the photoionization of a randomly oriented molecular beam if one assumes the intramolecular axis as quantization axis the spin-polarization vector follows. But nevertheless, pronounced electron-polarization effects have been found[8] in the photoionization of randomly oriented halogen molecules by unpolarized radiation. Both cases discussed for atoms exist for

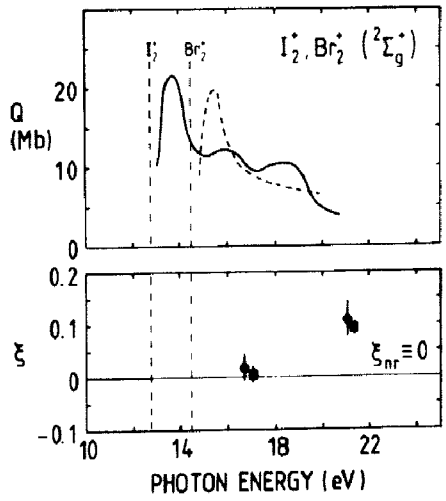

FIG. 14. Experimental results of the spin parameter ξ for photoelectrons leaving Br_2^+ (squares) and I_2^+ (circles) in their $^2\Sigma_g^+$ states[8] in comparison with the corresponding partial cross sections Q [38](Br_2 dashed, I_2 solid). The vertical lines indicate the adiabatic ionization thresholds.

molecular photoionization, too. Fig. 14 shows in the lower part the spin parameter ξ for photoelectrons leaving Br_2^+ (squares) and I_2^+ (circles) in their $^2\Sigma_g^+$ ionic state, where neither the ground neutral nor the final ionic state has any fine-structure splitting. The spin polarization, which occurs close to the photon energy where the cross section (Fig. 14 upper part) strongly decreases, is analogous to the well known Fano effect[1] in s-subshell ionization of alkali atoms. The dynamical spin parameters here are direct measure for the evidence of the spin-orbit interaction in the continuous spectrum.

Ionizing a π-orbital of halogens yields photoelectron spectra, which show a spin-orbit fine-structure splitting corresponding to the ionic total angular momentum 3/2 and 1/2 as in the rare-gas analogon. The behavior of spin polarizations and photoelectron intensities for the outermost orbitals of Br_2, I_2, CH_3Br and CH_3I is the most striking example studied in atomic and molecular photoionization with respect to the fact that photoelectron intensity data follow a certain theoretical prediction[37] - in our case the nonrelativistic model neglecting the influence of the spin-orbit

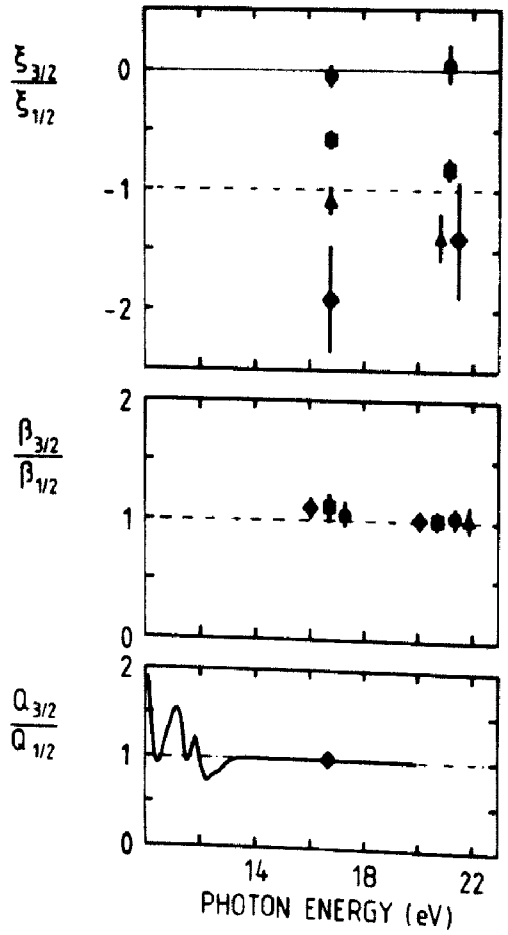

FIG. 15. Comparison of the ratios of the spin parameter ξ, asymmetry parameter β[8] and partial photoionization cross section Q[38] (for I_2 only) with the nonrelativistic predictions[37] (chain lines) for photoelectrons from the outermost orbitals of Br_2, I_2, CH_3Br, and CH_3I (squares, circles, triangles, and diamonds, respectively). The results correspond to photon energies of 16.85 and 21.22 eV.

interaction onto the molecular continuum states - whereas spin polarizations do not. Fig. 15 summarizes all experimental ratios of the spin parameter ξ, the asymmetry parameter β[8] and the partial cross section Q[38] for the spin-orbit components of these lone-pair orbitals. In all cases the ratio of β agrees with the theoretical prediction of +1 and the branching ratio $Q_{3/2}/Q_{1/2}$ (for I_2 only) is also identical to the statistical value over the energy range outside the threshold region. In contrast to this behavior of the differential cross section, the ratios of the spin parameters show a significant systematic deviation. While $\xi_{3/2}/\xi_{1/2}$ is close to -1 for CH_3Br (triangles) and not far from -1 for Br_2 (squares), it is zero for I_2 (circles), and tends to -2 for CH_3I (diamonds). In contrast to the cross sections, the spin polarizations are very sensitive to any phase shift of the continuum wave functions induced by the spin-orbit interaction. This, however, is stronger for heavier atoms in molecules than for lighter.

A very recent experiment of angular resolved photoelectron spectroscopy of free oriented CH_3I molecules has been performed for the first time.[9] CH_3I molecules in a supersonic beam have been oriented with respect to the molecular axis parallel to an external field by use of an electric hexapole in a "Stern-Gerlach" type analogous experiment. The photoelectrons ejected by vuv radiation in a region of very weak field (0.3 V/cm) from the lone-pair orbital at the iodine atom show a pronounced asymmetry in intensities depending on whether they are emitted parallel or antiparallel to the intramolecular axis. If the methyl group is directed toward the electron spectrometer, a photoelectron current I^+ is detected, if the iodine atom is directed, a current I^-. Fig. 16 shows the asymmetries I^-/I^+ measured for both spin-orbit components in the photoelectron spectrum and for two vuv photon energies (NeI and HeI light) as function of the focussing voltage in the hexapole.[9] The heights of the full points with error bars are roughly proportional to the degree of molecular orientation which has been estimated to be between 0.24 and 0.40. Comparing this degree of orientation with the asymmetry ratios found, the forward backward photoelectron-emission asymmetry parallel to the molecular axis must be a pronounced effect for a complete orientation of the molecules.

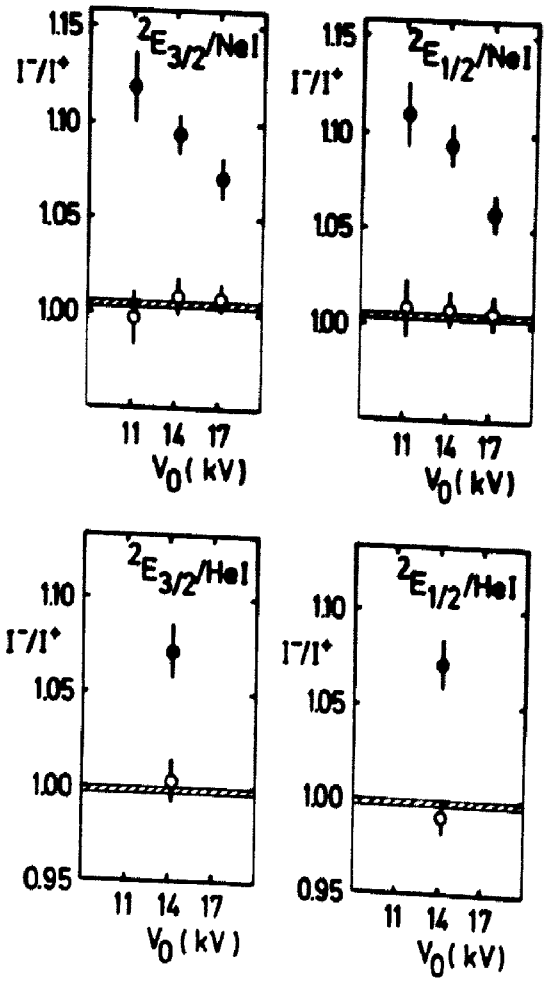

FIG. 16. Experimental results of the intensity asymmetry of photoelectrons emitted angular resolved parallel or antiparallel to the molecular axis of a free oriented CH_3I molecule (full points with error bars).[9] The open points and the dashed areas represent the corresponding results with a randomly oriented molecular beam showing the apparatus-related asymmetries.

PHOTOEMISSION FROM ATOMS ADSORBED ON SOLID SURFACES

Using circularly polarized synchrotron radiation at BESSY spin polarized photoemission from the valence orbitals of Xe and Kr atoms physisorbed on the Pt(111) single-crystal surface has been studied for normal light incidence and normal (angular resolved) emission. Two spin-resolved photoemission spectra[5,6] are shown in Fig. 17 for Kr and Xe monolayers adsorbed on Pt(111). The peak at lowest binding energy (1) has nearly complete negative spin polarization and corresponds to the $p_{3/2}|m_j| = 3/2$ hole state of the rare gas atoms, whereas peaks 2 and 3 are highly positive polarized ($|m_j| = 1/2$). These polarization values quantitatively correspond to the experimental results in the gas phase[3] (Fig. 2 middle part $\theta = 0$) except that for free atoms there is no ener-

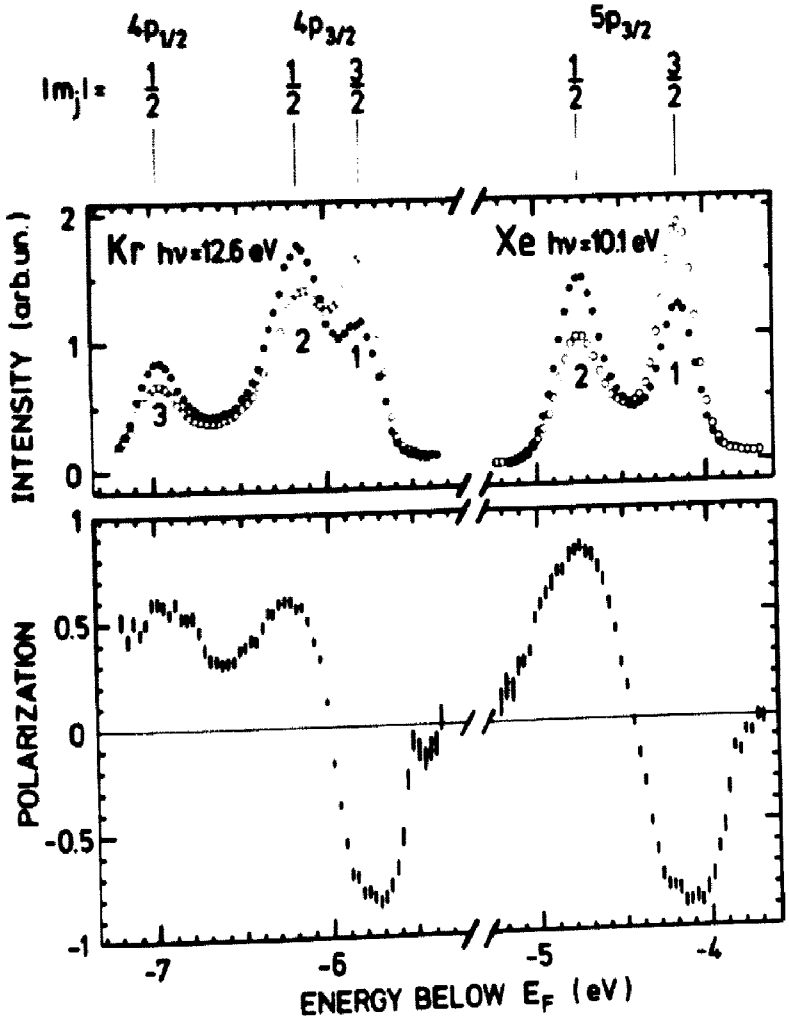

FIG. 17. Spin-resolved photoelectron spectra of Kr and Xe monolayers at full coverage on Pt(111) in normal photoemission.[5,6] Upper part, intensities scattered into the two counters 3 and 4 of the Mott detector (Fig. 3) as full and open circles. Lower part, photoelectron-spin polarization obtained from the count rates in the upper part, normalized to a complete circular photon polarization.

getic splitting of the m_j substates. These spin-polarization results confirm experimentally the peak assignment proposed in the literature[3,9] as shown in Fig. 17 which indicates that the m_j splitting is caused by lateral Xe-Xe interactions.

Fig. 18 gives two examples of spin-polarization data obtained for the different peaks in Fig. 17 plotted as function of the photon energy for an incommensurate hcp and a commensurate $\sqrt{3}$ layer of Xe. The polarization shows pronounced resonance structures which partly correspond with structures of the photoelectron intensities measured and shown in the upper part of Fig. 18. These structures which are discussed in more detail elsewhere[5,6] may partly be due

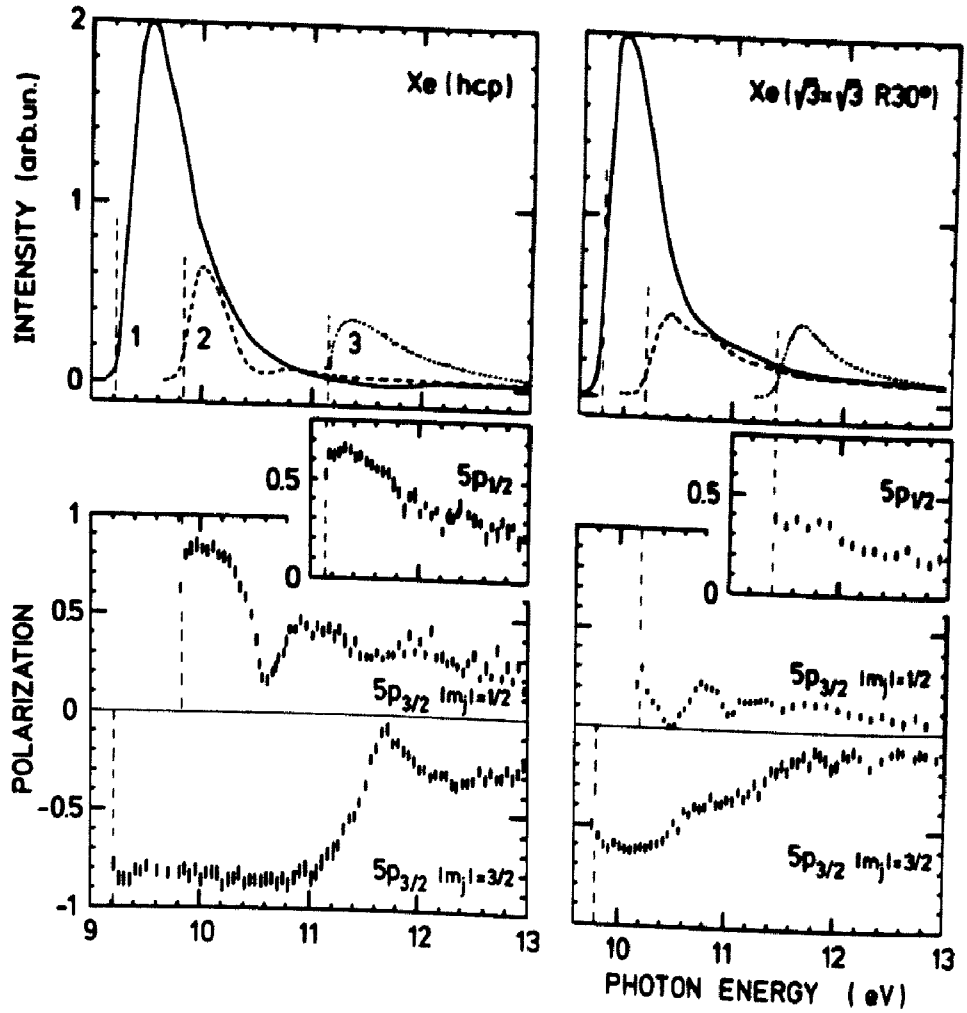

FIG. 18. Photoelectron intensities (upper part) and spin polarizations (lower part) of the Xe adsorbate photoemission peaks (normal emission) as function of the photon energies for hcp (incommensurate layer) and the $\sqrt{3}$ commensurate layer.[5,6] Peaks 1, 2, 3 are numbered within increasing binding energies (vertical dashed lines) corresponding to the rare gas hole states $5p_{3/2,1/2}$.

to atomic effects like autoionization resonances (the analogous spin parameter A of free xenon atoms measured[19] in comparison with theoretical curves[12,19,40] and the photoionization-cross section Q[19] are shown in Fig. 19) or Cooper minima or due to typical surface effects like electron diffraction patterns or resonances induced by the surface barrier. Further studies of different adsorbates on different substrates with different crystallographic structure and interatomic distances shall allow to answer these questions more quantitatively.

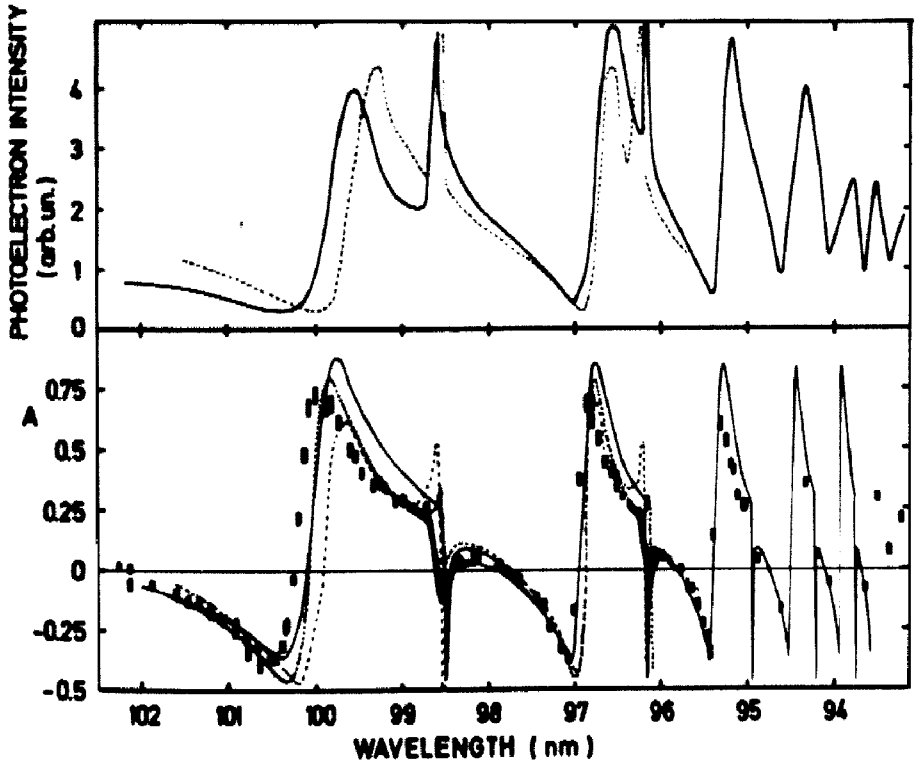

FIG. 19. Photoionization of Xe atoms in the autoionization range: (top) cross section, photoelectron intensity; (bottom) spin polarization parameter A. Experimental results (error bar rectangles lower part and full curve upper part[19]); theoretical curves: dashed[12], dotted[19,24], full[40].

OUTLOOK AND ACKNOWLEDGEMENT

It is the purpose of the angle- and spin-resolved photoelectron spectroscopy to find a set of non-redundant experimental data which characterize the photoeffect quantummechanically completely. This has been shown for atoms successfully. To build a quantitative bridge from the free atoms, via the free randomly oriented molecules up to the three dimensional crystal[7] will be the main topic of the angle- and spin-resolved photoemission studies in the future. Thus atomic physics can become an applied method to study and to understand more complicated systems like condensed matter. There is no doubt, that correlation effects studied in details for atoms play an important role there, too.

The author wishes to express his thanks to the coworkers Drs. A. Eyers, Ch. Heckenkamp, S. Kaesdorf, F. Schäfers, and G. Schönhense for the measurements performed and many intensive discussions. Support by the BMFT, DFG, and MPG is gratefully acknowledged.

REFERENCES

1. U. Fano, Phys. Rev. 178, 131 (1969)
2. U. Heinzmann, Appl. Opt. 19, 4087 (1980)
3. Ch. Heckenkamp, F. Schäfers, G. Schönhense, and U. Heinzmann, Phys. Rev. Lett. 52, 421 (1984)
4. Ch. Heckenkamp, F. Schäfers, and U. Heinzmann, 2. ECAMP Amsterdam 1985, book of abstracts
5. G. Schönhense, A. Eyers, U. Friess, F. Schäfers, and U. Heinzmann, Phys. Rev. Lett. in press (1985)
6. G. Schönhense, A. Eyers, U. Friess, F. Schäfers, and U. Heinzmann, Surface Science Symposium Obertraun (Austria) 1985, book of abstracts
7. A. Eyers, F. Schäfers, G. Schönhense, U. Heinzmann, H. P. Oepen, K. Hünlich, J. Kirschner, and G. Borstel, Phys. Rev. Lett. 52, 1559 (1984)
8. G. Schönhense, V. Dzidzonou, S. Kaesdorf, and U. Heinzmann, Phys. Rev. Lett. 52, 811 (1984)
9. S. Kaesdorf, G. Schönhense, and U. Heinzmann, Phys. Rev. Lett. in press (1985)
10. Ch. Heckenkamp, doctoral thesis, F. University of Berlin (1984), unpublished
11. N. A. Cherepkov, Zh. Eksp. Teor. Fiz. 65, 933 (1973) (Sov. Phys. JETP 38, 463 (1974))
12. C. M. Lee, Phys. Rev. A 10, 1598 (1974)
13. U. Heinzmann, G. Schönhense, and J. Kessler, Phys. Rev. Lett. 42, 1603 (1979) and J. Phys. B 13, L 153 (1980)
14. G. Schönhense, Phys. Rev. Lett. 44, 640 (1980)
15. B. Brehm, Z. Phys. 242, 195 (1971)
16. A. Eyers, Ch. Heckenkamp, F. Schäfers, G. Schönhense, and U. Heinzmann, Nucl. Instrum. Meth. 208, 303 (1983)
17. K. Jost, J. Phys. E 12, 1006 (1979)
18. J. Kessler, "Polarized Electrons", Springer, Berlin (1976)
19. U. Heinzmann, J. Phys. B 13, 4353 (1980)
20. G. Schönhense, doctoral thesis, University Münster (1981), unpublished
21. K. N. Huang, W. R. Johnson, and K. T. Cheng, At. Data Nucl. Data Tabl. 26, 33 (1981)
22. N. A. Cherepkov, J. Phys. B 12, 1279 (1979)
23. K. N. Huang, W. R. Johnson, and K. T. Cheng, Phys. Rev. Lett. 43, 1658 (1979)
24. J. Geiger, Z. Phys. A 282, 129 (1977) and private communication (1979)
25. H. Klar, J. Phys. B 13, 3117 (1980)
26. K. N. Huang and A. Starace, Phys. Rev. A 21, 697 (1980)
27. B. Brehm, Z. Naturforsch. 21a, 196 (1966)
28. B. Brehm and K. Höfler, Phys. Lett. 68A, 437 (1978)
29. K. Höfler, PhD-thesis, University Hannover (1979), unpublished
30. F. Schäfers, G. Schönhense, and U. Heinzmann, Z. Phys. A 304, 41 (1982)
31. G. Schönhense, F. Schäfers, Ch. Heckenkamp, U. Heinzmann, and A. M. Baig, J. Phys. B 17, L 771 (1984)

32. G. Schönhense and U. Heinzmann, Phys. Rev. A 29, 987 (1984)
33. Y. S. Kim, R. H. Pratt, A. Ron, and H. K. Tseng, Phys. Rev. A 22, 567 (1980)
34. F. Keller and F. Combet-Farnoux, J. Phys. B 12, 2821 (1979) and 15, 2657 (1982)
35. K. Ivanov, S. Yu. Medvedev, and V. A. Sosnivker, unpubl. Report No 615 (1979) A. F. Ioffe Phys. Techn. Inst. Leningrad
36. U. Heinzmann, J. Phys. B 13, 4367 (1980)
37. N. A. Cherepkov, J. Phys. B 14, 2165 (1981)
38. J. H. Carver and J. L. Gardner, J. Quant. Spectrosc. Radiat. Transfer 12, 207 (1972)
39. K. Horn, M. Scheffler, and A. M. Bradshaw, Phys. Rev. Lett. 41, 822 (1978)
40. W. R. Johnson, K. T. Cheng, K. N. Huang, and M. LeDourneuf, Phys. Rev. A 22, 989 (1980)